Force Generation by Actin Polymerization II: The Elastic Ratchet and Tethered Filaments

Alex Mogilner* and George Oster†
*Department of Mathematics and Center for Genetics and Development, University of California, Davis, California 95616; and
†Departments of Molecular and Cellular Biology and Environmental Science, Policy and Management,
University of California, Berkeley, California 94720

ABSTRACT The motion of many intracellular pathogens is driven by the polymerization of actin filaments. The propulsive force developed by the polymerization process is thought to arise from the thermal motions of the polymerizing filament tips. Recent experiments suggest that the nucleation of actin filaments involves a phase when the filaments are attached to the pathogen surface by a protein complex. Here we extend the "elastic ratchet model" of Mogilner and Oster to incorporate these new findings. We apply this "tethered ratchet" model to derive the force-velocity relation for *Listeria* and discuss relations of our theoretical predictions to experimental measurements. We also discuss "symmetry breaking" dynamics observed in ActA-coated bead experiments, and the implications of the model for lamellipodial protrusion in migrating cells.

INTRODUCTION

Cell crawling is an important phenomenon that drives cellular and developmental processes as diverse as morphogenesis and metastasis (Bray, 2001; Mitchison and Cramer, 1996). Cell locomotion is directional, ATP-consuming, and is associated with actin polymerization. It is a complex process, coupling protrusion of the cell's leading edge, contraction of the cytoskeleton, and dynamic graded adhesion (Bray, 2001). The phenomenon of lamellipodial protrusion—motile appendages of rapidly migrating simple shaped cells—is one aspect of cell movement where our understanding is the most advanced (Beckerle, 1998; Borisy and Svitkina, 2000; Cameron et al., 2000; Pantaloni et al., 2001; Pollard et al., 2000). However, involvement of the actin machinery in many aspects of cellular behavior, the functional multiplicity and redundancy of actin accessory proteins, and the requirement of an intact cell plasma membrane have frustrated the interpretation of experiments.

Therefore, research has focused on simplified model systems for eukaryotic cell motility, in particular, the bacterial pathogen, *Listeria monocytogenes* (Tilney and Portnoy, 1989). These bacterial cells have been instrumental in identifying essential factors in motility and in developing biophysical assays for motion analysis (Beckerle, 1998). The bacterium is able to assemble the host cell's actin into a cometlike tail made up of oriented, cross-linked networks of actin filaments, with their barbed (growing) ends oriented toward the bacterial surface (Tilney and Portnoy, 1989). *Listeria* moves through the host cytoplasm rapidly, with velocities of the order of tenths of a micron per second (Cameron et al., 2001). Actin polymerizes at the bacterial surface with the same rate as that of the bacterial cell propulsion, suggesting that the actin growth drives the bacterium forward (Theriot et al., 1992).

Long ago, it was suggested that actin polymerization itself generates a protrusive force (Condeelis, 1993; Cortese et al., 1989; Hill and Kirschner, 1982). This was confirmed experimentally (Miyata et al., 1999). The exact mechanism of this force generation is still debated. Initially, Peskin et al. (1993) suggested a Brownian ratchet (BR) mechanism. According to this model, the bacterium thermally fluctuates away from the rigid actin polymer, creating a gap between the polymer tip and the cell surface. Actin monomers intercalate into this gap and assemble onto the tip, thereby inhibiting the bacterium from diffusing backward. Even when a load force is applied to the bacterium, Brownian motion can still create a sufficient gap, and so the cell movement is biased forward. This model predicted that the bacterial velocity should depend on its diffusion coefficient, and thereby on its size. Experiments failed to show such a size dependence, and so the BR model was developed further by Mogilner and Oster (1996), who suggested an ''elastic Brownian ratchet'' (EBR) mechanism, whereby thermal bending undulations of a semi-stiff actin fiber, rather than bacterial diffusion, creates the polymerization gap, and the elastic force of the growing filaments pushes the bacterium forward. These models were based on the behavior of individual actin filaments. Gerbal et al. (2000) developed a continuum model of *Listeria* propulsion relying on the elastic shear stress developed by growth of the actin meshwork at the cell surface. In this model, the macroscopic elastic forces in the actin meshwork are considered, although the question of the molecular mechanism of the elastic stress generation is not specified. An ultimate model, still pending, would be a combination of a macroscopic viscoelastic model of the actin tail, combined with the microscopic ratchet model of the growing edge of the network that provides boundary conditions for the macroscopic model.

Finally, an alternative hypothesis posits the existence of an Ena/VASP-mediated ratcheting mechanism, driven by the

Submitted March 18, 2002, and accepted for publication November 11, 2002.

Address reprint requests to George Oster, 201 Wellman Hall, Berkeley, CA 94720. Tel.: 510-642-5277; Fax: 510-642-7428; E-mail: goster@nature.berkeley.edu.

0006-3495/03/03/1591/15 $2.00

free energy of monomer addition at the actin/cell interface (Laurent et al., 1999). A recent model suggests a possible motorlike mechanism based on the modulated binding interaction between actin filaments and VASP fueled by the hydrolysis of actin-bound ATP (Dickinson and Purich, 2002). More detailed measurements are necessary to distinguish between the EBR model and a specialized motorlike mechanism as a force-generating process. Here we modify the original EBR model taking into account transient binding at the actin/cell interface. We show that this model fits the available data and generates testable predictions for future experiments.

The only protein on the surface of *Listeria* required for motility is ActA (Cameron et al., 1999). Indeed, polystyrene beads coated with ActA and WASP are capable of forming actin tails and moving in cytoplasmic extracts (Yarar et al., 1999). Loisel et al. (1999) demonstrated that, in addition to actin monomers and ATP, only a handful of proteins in cytoplasmic extracts is essential for bacterial propulsion. Of those, the Arp2/3 protein complex nucleates nascent actin filaments. Essential capping proteins limit actin growth. Finally, the turnover of actin is maintained at a high level by ADF/cofilin depolymerization factors. The VASP protein, although not essential, increases the rate of cell movement 10-fold. The cross-linking protein α-actinin, also not essential, stabilizes the movement. Finally, Loisel et al. (1999) proved that no myosin is required for the bacterial propulsion.

Though still not confirmed in all details, the following dendritic nucleation model explains much of the geometrical organization of actin-based propulsion (Borisy and Svitkina, 2000; Cameron et al., 2000; Pantaloni et al., 2001; Pollard et al., 2000). Polystyrene beads coated with ActA grow an actin tail consisting of but a few filaments, which allows observing the structure of the actin network in detail (Cameron et al., 2001). ActA activates the Arp2/3 protein complex (Welch et al., 1998). This involves the Ena/Mena/VASP family of proteins, which may bind directly simultaneously to both ActA and F-actin, and thus connects the actin tail to the bacterium (Boujemaa-Paterski et al., 2001; Laurent et al., 1999). Activated Arp2/3 complex mediates branching of the nascent filaments from the sides or tips of the existent actin fibers (Egile et al., 1999). The actin filament arrays in comet tails behind latex beads coated with ActA have a dendritic organization with Arp2/3 localizing to Y-junctions, just as it does in lamellipodia of motile eukaryotic cells (Cameron et al., 2001). The asymmetric structure of the Y-junctions in actin tails suggests that capping activity terminates the elongation of the barbed ends (Cameron et al., 2001).

There are many similarities between actin dynamics in *Listeria* and in the lamellipodia of some rapidly locomoting eukaryotic cells (Cameron et al., 2000). However, the mechanism of VASP's interaction with the cell membrane remains uncertain (Bear et al., 2001). In lamellipodia, the WASP/Scar protein family activates Arp2/3 to nucleate actin filaments (Machesky et al., 1999). Some observations suggest that filaments are linked transiently to the cell membrane through N-WASP (Pantaloni et al., 2001). Similarly, in the bacterial pathogen *Shigella*, the IcsA protein plays the role of ActA and interacts with N-WASP, which in turn interacts with Arp2/3 and actin. (More specifically, N-WASP may be coupled to actin through Arp2/3 and to the cell membrane involving the small GTPase Cdc42 and/or PIP_2 (Rohatgi et al., 1999).

Actin-based movement is the mechanical phenomenon, and the mechanical aspects of it are the focus of our attention in this paper. One of the most important recent discoveries about the actin propulsion is the proof (after some earlier indications, see (Olbris and Herzfeld, 2000)) that the actin tail is attached to the surface of the pathogens (Kuo and McGrath, 2000; Noireaux et al., 2000) and beads (Cameron et al., 2001). This was shown by high resolution trajectory analysis (Kuo and McGrath, 2000), which demonstrated that the effective diffusion coefficient of the bacterium is a few orders of magnitude less than that of the free pathogens. Noireaux et al. (2000) used an optical trap to measure the force required to separate the bacterial cell from the actin tail, which turned out to be greater than 10 pN. Finally, Cameron et al. (2001) used electron microscopy to observe that actin filaments of the branching network are transiently attached to the surface of the bead.

F-actin attachment to the bacteria or beads seems to ensure stable and persistent movement. However, the question arises: how can EBR-type models, which rely on the existence of a gap between undulating filaments and the cell surface, coexist with the fact that the filaments attach to the surface? Our answer to this question is that the filaments attach to the bacterial surface transiently. Nascent filaments are associated with the protein complexes on the surface, but then they dissociate and grow freely, until finally they are capped and lose contact with the surface. During this process, the attached fibers are in tension and resist the forward progress of the bacterium/bead. At the same time, the dissociated fibers are in compression, and generate the force of propulsion. In ''The Model'' section, we derive and analyze the model equations. We demonstrate quantitatively that a few straightforward assumptions about the nature of the molecular bonds between the F-actin and surface and the nature of the polymerization force generation explain most of the observations on steady-stable propulsion. In the ''Results'' section, we compare the model predictions with experimental observations and measurements of Cameron et al., (1999, 2001). In the ''Stochastic Model'' section, we consider a stochastic model of actin-based propulsion that incorporates fluctuations in velocity. This will explain the symmetry breaking phenomenon observed in actin meshworks. The model's conclusions and its implications to the lamellipodial protrusion are discussed in the ''Discussion'' section.

DESCRIPTION OF RELEVANT OBSERVATIONS AND MEASUREMENTS

The plastic beads in cytoplasmic extract coated with ActA move with rates of 10–100 nm/s (Cameron et al., 2001). Bacteria often move faster in vivo, up to a micron per second. The density of ActA coating and the degree of dilution of the cytoplasmic extract do not have noticeable effects on the propulsion velocity (Cameron et al., 1999, 2001). In the experiments of Cameron et al. (2001), just a few filaments are sufficient to propel the movement of beads 0.2 and 0.5 μm in diameter. There is a correlation between the size and the velocity of the beads: smaller beads move slower (Cameron et al., 1999, 2001), and beads 0.05 μm in diameter do not move persistently, and they often lose their connection with the actin filaments (Cameron et al., 2001). Some of the actin filaments appear curved and twisted in the electron micrographs with corresponding radii of curvature 50–100 nm (Cameron et al., 2001). The curved filaments are restrained by at least two cross-links. The length of individual fibers in the branching networks appears to be tens to few hundreds nm. All these observations place stringent constraints on the theory. We will argue that, if the model's predictions agree with the experimental results, then the model is likely to be at least partially true, despite the fact that there are many unknown parameters.

THE MODEL

The EBR mechanism for force generation via polymerization depends on the fluctuations of filaments against a load surface, here the surface of a bacterium or of a bead. However, inasmuch as actin filaments are nucleated when they are tethered to the load surface, they can only generate a protrusive force after they detach. Therefore, we formulate a two-compartment model consisting of attached and detached filaments, shown in Fig. 1. Only the latter are ''working'' filaments, i.e., force generating; this puts the attached filaments into tension, inasmuch as both populations are anchored in their distal region to the surrounding cytoskeletal network.

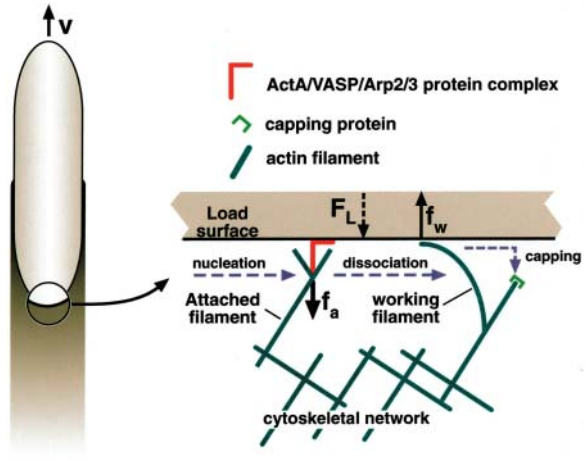

FIGURE 1 Sketch of the model. Attached filaments (*straight*) are nucleated at rate n. They dissociate with rate δ and become ''working'' filaments (*bent*). These, in turn, are capped at rate κ. Force balance: the polymerization ratchet force, f_w, generated by the working filaments is balanced by the force of attachment, f_a, and load force, $F_L = F_{ext} + \zeta V$.

Model equations

The model consists of i), dynamic equations for the numbers of actin filaments near the surface, ii), a force-balance equation, and iii), constitutive relations describing force and dissociation rate.

Actin dynamics

The dynamic variables and parameters of the model are (Tables 1 and 2):

$a(t)$ [#] = number of filaments attached to the surface (via the ActA, VASP, etc.).
$w(t)$ [#] = number of ''working'' filaments, i.e., filaments not attached to the surface that are polymerizing and generating force.
n [1/s] = nucleation rate of attached filaments. We assume that the nascent filaments are nucleated and branch out from the tips or sides of the existing attached fibers.
δ [1/s] = filament dissociation rate.
κ [1/s] = capping rate of growing filaments.

The dynamics of the two filament populations obey the following system of equations.

$$\text{Attached filaments: } \frac{da}{dt} = \underset{\text{Nucleation}}{n} - \underset{\text{Dissociation}}{\delta \cdot a} \tag{1}$$

$$\text{Working filaments: } \frac{dw}{dt} = \underset{\text{Dissociation}}{\delta \cdot a} - \underset{\text{Capping}}{\kappa \cdot w}\,. \tag{2}$$

The molecular mechanisms of actin filament dynamics are not known in detail; therefore, we formulate a model as simple and general as possible. Some of the more detailed plausible mechanisms, such as an autocatalytic production of

TABLE 1 Model variables

Symbol	Definition	Units
a	Number of attached filaments	[#]
w	Number of working filaments	[#]
t	Time	[s]
f_w	Polymerization ratchet force generated by a single filament	[pN]
f_a	Attachment force per filament	[pN]
F_L	Load force	[pN]
V	Velocity of the load (cell or bead)	[nm/s]
δ	Effective dissociation rate	[s^{-1}]

TABLE 2 Model parameters

Symbol	Definition	Value & Units
n	Nucleation/branching rate	~10 [#/s]
κ	Capping rate	≈0.5 [/s]
δ_0	Free dissociation rate	≈0.5 [/s]
V_{max}	Free polymerization rate	~500 [nm/s]
V_{dep}	Free depolymerization rate	≈2.2 [nm/s]
l	Average length increment of actin filament in the direction of growth after one act of assembly	≈2.2 [nm]
k_BT	Thermal energy	≈4.1 [pN·nm]
x_b	Effective length of the attachment bond	0.4 nm
f_b	Effective strength of the attachment bond	10 pN
k	Spring coefficient of the transducer spring	1 pN/nm

filaments at the surface of the bead (M.F. Carlier, personal communication), give equations slightly different from ours. However, in the Appendix, we show that, remarkably, these equations give the same result as our simple equations. Also in the Appendix, we discuss filament turnover and mechanics in greater detail. Our assumption that the nucleation rate is independent of the number of filaments is based on the assumption that the number of nucleation sites, not the number of filaments, is constant and rate limiting.

Force balance

Let f_w and f_a be the force exerted by a working or attached filament, respectively, and F_{ext} be the external conservative force exerted on the cell by, say, a laser trap. The viscous drag force on the cell is ζV, where ζ is the drag coefficient and V the cell velocity. The force balance is shown in Fig. 1, where the sign convention is taken as positive when the load and attachment force oppose the movement, and a positive working force is in the direction of propulsion:

$$\underset{\text{Total load force}}{F_L} + \underset{\text{Attached filaments}}{f_a \cdot a} = \underset{\text{Working filaments}}{f_w \cdot w}, \tag{3}$$

where $F_L = \zeta V + F_{ext}$ is the total dissipative and conservative load force. We assume that the actin tail is cross-linked firmly into the cytoskeleton of the host cell (or cytoplasmic extract) and/or attached to the coverslip. Thus, the force on the actin tail does not enter the force-balance equation. (We discuss the role of the elastic recoil of the tail near the bacterium/bead surface below.)

Constitutive relations

The forces f_w and f_a, as well as the effective dissociation rate, are functions of the velocity of the bacterium, V. Therefore, to complete the model, we must specify these functions. A force-velocity relation for the interface between the actin tail network and the load surface gives the dependence of the polymerization ratchet force on the velocity of propulsion. Previously, we have demonstrated that, in the biologically relevant regime, the force-velocity relation for the single filament has the form (Mogilner and Oster, 1996):

$$V = V_{max} \exp[-f_w l/k_BT] - V_{dep}, \tag{4}$$

where $V_{max} = k_{on} \cdot l \cdot M$ is the free polymerization velocity and $V_{dep} = k_{off} l$ is the depolymerization velocity. Here k_{on} is the rate of monomer assembly, M is the effective concentration of G-actin monomers available for polymerization, and k_{off} is the rate of monomer's disassembly. l is the amount a filament grows by the addition of one monomer. Because the filament is a double helix, l is equal to half the size of an actin monomer times the average cosine of the angle between the filament's orientation and the direction of motion. In the absence of the load force, filaments would grow with the rate $V = V_{max} - V_{dep}$. The BR models assume that the depolymerization rate does not depend on the load, but the free polymerization rate is decreased by the exponential Boltzmann factor, where $f_w l$ is the work done by a filament against the load during one act of assembly. k_B is Boltzmann's constant, and T the absolute temperature; k_BT is the unit of thermal energy. Gerbal et al. (2000) demonstrated that the rate of growth of the actin meshwork is decreased, in comparison with that of a single filament, due to elastic recoil under load by a factor of the order of $(1 + (F_L/YA))$, where Y is the compression modulus of the actin tail, A is the cross-sectional area of the load surface, and F_L is the load force. For *Listeria* operating in the physiological range, $YA \sim 1$ nN (Gerbal et al., 2000), whereas $F_L < 200$ pN (McGrath et al., 2003); therefore, the elastic recoil factor is ≈1, so that this effect does not introduce a significant correction to Eq. 4. Therefore, we will use Eq. 4 to relate the polymerization force, f_w, to the propulsion velocity, V.

When the attachment is not loaded, dissociation takes place spontaneously with rate δ_0. With a constant force, f, applied to the molecular link, the effective dissociation rate can be approximated by the formula: $\delta = \delta_0 \cdot g(f/f_b) \cdot \exp[f/f_b]$ (Evans, 2001; Evans and Ritchie, 1999). Here the preexponential factor, g, is defined by the specific form of the effective potential associated with the molecular link. If the link corresponds to a sharp barrier at a fixed location x_b along the dissociation pathway, then $g(f/f_b) \approx 1$. If the link is modeled by a deep harmonic well, then $g(f/f_b) \approx f/f_b$. Evans (2001) treats several other limiting cases; however, the exponential factor always dominates the preexponential factor, which has little influence on the model's behavior (Evans and Ritchie, 1999). Thus, we will use the following model as the approximation for the dissociation rate:

$$\delta \approx \delta_0 \cdot \exp(f/f_b). \tag{5}$$

The force applied to an attachment bond is not constant. Before attachment, the molecular link between the filament and the surface is stress free. Then, as the load continues to

move relative to the actin tail, the link is deformed, and a tensile force develops. Mechanically, the actin meshwork of the tail, the individual attached filament, and the proteins linking the filament to the surface are equivalent to springs acting in series. We shall assume that one of these effective springs is linear and much more flexible than the others. Note that the most flexible element in the protein chain is not necessarily the same as the molecular link, although we assume that the link is the element that breaks most easily. The reason for this assumption is that we estimate the attachment force to be of the order of 10–30 pN (see below). Much greater forces are required to break actin filaments (van Oudenaarden, personal communication). On the other hand, individual attached filaments are likely to be the most flexible element inasmuch as both actin binding proteins, and molecular links with the surface cannot be deformed by tens of nanometers. Denote by k the spring coefficient of this transducer spring. If the load moves with constant velocity V, then at time t after the instant of attachment, the transducer spring extension is equal to $V{\cdot}t$, and the force applied to the molecular link is $f = k{\cdot}V{\cdot}t$. Thus, the force applied to the attachment is velocity-dependent, and grows at the constant rate $k{\cdot}V$. This simple relation is crucial for the model. By a similar argument, the dissociation rate is time and velocity dependent:

$$\delta(V,t) \approx \delta_0 \cdot \exp[kVt/f_b]. \tag{6}$$

Next, we compute the probability of bond failure. The probability of the tether link breaking in the time interval $(t, t + dt)$ is the product of the probability of failure within this interval, $\delta(t)dt$, times the probability that there was no failure in the time interval $(0, t)$, $\exp[-\int_0^t \delta(t')dt']$: $p(t) = \delta(t)\cdot \exp[-\int_0^t \delta(t')dt']$. The average time from the attachment's formation to its failure is $\langle t\rangle = \int_0^t t' \cdot p(t')dt'$. The effective dissociation rate is $\delta = 1/\langle t\rangle$. The average force applied to the attachment, $\langle f\rangle = \int_0^t f(t')\cdot p(t')dt' = kV\int_0^t t' \cdot p(t')dt'$. Therefore, we can define the average attachment force in Eq. 3 as

$$f_a = \langle f\rangle = kV\langle t\rangle. \tag{7}$$

Let us introduce the velocity scale, $V_0 = f_b\delta_0/k$. V_0 is the propulsion velocity at which the attachment bond stretches to its length, x_b, over the characteristic bond lifetime, $1/\delta_0$. Roughly speaking, when the speed of the load is less than V_0, then the molecular links are weakly deformed, and the bonds break with the free dissociation rate. At greater speeds, the links stretch beyond their yield point faster than their average lifetime, and the effective dissociation rate increases, becoming velocity dependent. Denote the dimensionless velocity $v \equiv V/V_0$. Then, the following are the velocity dependencies of the average dissociation rate and attachment force:

$$\delta(v) = \delta_0/\omega(v),$$
$$f_a(v) = f_b \cdot \omega(v) \cdot v,$$
where $$\omega(v) = \int_0^\infty dx \cdot x \cdot \exp\left[vx + \frac{1-e^{vx}}{v}\right]. \tag{8}$$

Note, that function $\omega(v)$ has the following asymptotic behavior:

i. If $v \ll 1$, $\omega(v) \approx 1$.
ii. If $v \gg 1$, $\omega(v) \approx \ln(v)/v$.

i means that if the movement is slow, $V \ll V_0$, then $\delta \approx \delta_0$; that is, the effective dissociation rate is equal to the free dissociation rate, and $f_a \approx f_b{\cdot}(V/V_0)$ (i.e., the attachment force is proportional to the rate of propulsion). In the opposite limiting case of fast propulsion (ii), $V \gg V_0$, $\delta \approx \delta_0{\cdot}v/\ln(v)$; that is, the effective dissociation rate increases with the load velocity in a sublinear way, and $f_a \approx f_b \cdot \ln(v)$, so that the detachment force increases slowly.

Equations 1–4 and 8 constitute a self-consistent system of equations. They allow us to estimate the rate of propulsion and derive the force-velocity relation.

Analysis

We investigate the model's behavior in the case of the steady propulsion with a constant rate. Actin dynamics Eqs. 1 and 2 have the following solution:

$$a(v) = n/\delta, \quad w(v) = n/\kappa. \tag{9}$$

Note that the ratio of the number of the working to attached filaments does not depend on the nucleation rate; this will have important biological implications as we discuss below.

Substituting the force-balance equation (3) into the force-velocity relation (4), we obtain:

$$V = V_{max}\exp[-l(f_a(a/w)+(F_L/w))/k_BT] - V_{dep}. \tag{10}$$

Using Eq. 8 for the attachment force and dissociation rates, the last equation can be rewritten in the form:

$$V = V_{max}\exp[-l(f_b v\omega^2(v)(\kappa/\delta_0)+(F_L\kappa/n))/k_BT] - V_{dep}. \tag{11}$$

We introduce the following four dimensionless parameters, which determine the model's behavior:

$\varepsilon_1 = (f_b l/k_BT)(\kappa/\delta_0)$: work done per working filament in breaking an attachment.
$\varepsilon_2 = (V_{max}/V_0)$: free polymerization velocity.
$\varepsilon_3 = (V_{dep}/V_0)$: free depolymerization velocity.
$\varepsilon_4 = (F_L l/k_BT)(\kappa/n)$: work performed on the load per working filament.

Using these definitions, Eq. 11 can be rewritten in the dimensionless form:

$$v = \varepsilon_2\exp[-\varepsilon_1 v\omega^2(v) - \varepsilon_4] - \varepsilon_3. \tag{12}$$

Estimates of the model parameters

The values of the five dimensional model parameters V_{dep}, l, k_BT, x_b, and f_b are known from the literature, and tabulated in Table 2. The values of the five remaining parameters are unknown: free polymerization rate, V_{max}; nucleation/branching rate, n; capping rate, κ; transducer spring constant, k; and free dissociation rate, δ_0. Therefore, we must estimate their values using the results of the experimental observations.

V_{max}

The free polymerization rate is proportional to the concentration of G-actin available for polymerization. This concentration is of the order of tens of micromolar (Pollard et al., 2000), and the corresponding order of magnitude of the free polymerization rate is hundreds of nanometers per second. (The G-actin available for polymerization includes both unsequestered ATP-G-actin, and ATP-G-actin sequestered by profilin. Whereas the former concentration is very low, the latter concentration is in the tens of micromolar range.)

κ

The capping rate can be estimated from the observation that the length of the actin fibers in the electron micrographs of Cameron et al. (2001) is tens to hundreds of nanometers. Assuming that capping terminates the filament's growth, the average length of actin filaments must equal the ratio (V/κ). The observed velocity of the beads is tens–hundreds nm/s, so $\kappa \sim 1$/s. We will use the value $\kappa = 0.5$/s. Note that the polymerization ratchet model predicts that actin filaments generate force effectively if the length of the filament tips (i.e., the distance from the barbed end to the first cross-link) is limited by a few tens of nanometers from below, and a few hundred nm from above. Shorter filaments are too stiff, and do not bend enough to create the necessary gap. Longer filaments are too flexible, and could be buckled by a load force less than the stall force.

n

The nucleation/branching rate can be estimated using the result that the total number of filaments near the surface of the bead (cell) is $\sim$10 (100) (Cameron et al., 2001; Kuo and McGrath, 2000). Assuming that the number of dissociated filaments is of the same order of magnitude as the total number of filaments, we estimate the order of magnitude of the nucleation/branching rate as $\sim$10 (100) filaments per second in the case of the bead (cell).

k

The transducer spring constant is determined by the weakest spring in the chain of proteins connecting actin meshwork of the tail and the surface of the load. This could be the attached actin filament itself. The effective spring constant corresponding to a bending filament 200-nm long is $\sim$0.1 pN/nm (Mogilner and Oster, 1996). However, if the filament remains attached for a significant time while the load continues to move, then the filament would be bent in the direction of propulsion, and further movement of the load would stretch the filament longitudinally. The corresponding time is $\sim$1 s (a displacement of the filament tip of a few tens of nanometers taking place over $\sim$1 s would completely stretch a filament of characteristic length and orientation). Below we argue that the filaments attached for times of order seconds. The effective spring constant corresponding to the longitudinal stretching of F-actin is very large, of the order of tens pN/nm (Kojima et al., 1994). In this paper we use the intermediate value $k = 1$ pN/nm. It is possible that the weakest spring corresponds to one of the actin-binding proteins linking actin fibers to the surface. The characteristic scale of the elastic constant of such protein spring is also 1 pN/nm (Howard, 2001) (see the Appendix for further discussion).

δ_0

The free dissociation rate is estimated as follows. If this rate is much greater than the capping rate, then the number of the attached filaments, a, is very small in comparison with the number of the working filaments, w. For example, if $\delta_0 = 5$/s, then $\delta_0/\kappa = 10$, and $a/w \approx \kappa/\delta_0 = 0.1$. However, if the total number of filaments near the bead surface is $\sim$10 (Cameron et al., 2001), then the number of attached filaments is $\sim$1. In this case, the stochastic nature of the actin dynamics would lead to frequent detachment of the bead from the actin tail and disruption of stable propulsion; this does not happen often. (When the bead is <0.05 μm in diameter, then the total number of filaments is $\sim$1, and the bead does lose its connection to the tail and does not move persistently (Cameron et al., 2001).) On the other hand, if the free dissociation rate is much less than the capping rate, then the number of the attached filaments, a, is much greater, than the number of the working filaments, w. In this situation, the attachment between the tail and the bead would be very firm, but the dissociated filaments would be compressed so much that they would be either stalled or buckled, and propulsion would cease. For example, consider the case when $\delta_0 = 0.1$/s. Analysis based on the numerical solution of Eq. 12 shows that, in this case, the effective dissociation rate increases $\sim$12-fold, to $\delta \approx 1.2$/s. Then, on the average, the transducer spring is stretched by $V/\delta \sim 50$ nm before detachment, and the average resistance force per attached filament is $f_a \approx k\cdot(V/\delta)/2 \sim 25$ pN. In this situation, $a/w \approx \kappa/\delta \approx 0.4$. In the absence of the external load, the average stall force per working filament, $f_w \approx f_a\cdot(a/w) \approx 10$ pN. At the observed rate of propulsion, this force would both stall and buckle a working filament. These arguments indicate that

stable and fast locomotion would be possible if the order of magnitude of the free dissociation rate is 1/s. (Indeed, this is the scale of the dissociation rate for some actin binding proteins (Howard, 2001).) In this paper, we use the value $\delta_0 = 0.5$/s.

Additional experiments supporting our estimates are the recent observation by van Oudenaarden (personal communication) that lipid vesicles coated with ActA grow actin tails and move similar to *Listeria*. Some filaments transiently associate with the vesicle surface, and the corresponding force of dissociation is of the order of tens of piconewtons per filament. This estimate does not allow one to calculate the free dissociation rate and effective spring constant separately, but our calculations below predict the force per attached filament is of the same order of magnitude.

RESULTS

Movement of ActA-coated beads

Cameron et al. (2001) coated latex beads with the *Listeria*-derived protein, ActA, and observed the actin comet tails that grew from, and propelled, the bead. Here we use the model to describe the movement of these beads. We solve Eq. 12 using the values of the model parameters listed in Table 2. For these values the viscous load is in the piconewton range, and thus is negligible in comparison with the actin-generated forces, thus $F_L \approx 0$. The velocity scale is $V_0 = 5$ nm/s, and the values of the four dimensionless model parameters are: $\varepsilon_1 \approx 5.4, \varepsilon_2 \approx 105, \varepsilon_3 \approx 0.5$, and $\varepsilon_4 \approx 0$. The numerical solution of Eq. 12 in this case is illustrated in Fig. 2 (see Appendix). The right-hand side of Eq. 12 is a decreasing function of the velocity at values of $v < 4$, because in the ''slow'' regime the dissociation rate is constant, whereas the force of attachment that resists the working filaments is proportional to the velocity. In the ''fast'' regime, when $v > 4$, the force of attachment increases with velocity more slowly than the dissociation rate, so that the corresponding resistance force per working filament decreases with velocity as $\sim v/ln^2(v)$. Therefore, for $v > 4$, the right-hand side of Eq. 12 is a slowly increasing function of the velocity.

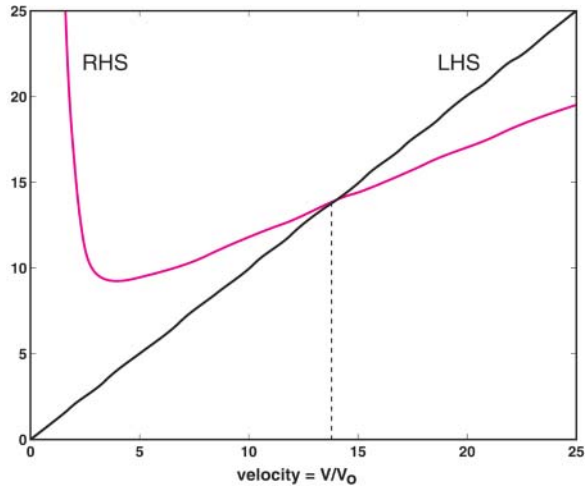

FIGURE 2 The right-hand side of Eq. 12 (*curve*) is plotted as the function of the dimensionless velocity, v. The left-hand side corresponds to the straight line. The intersection gives the steady-state value of v. The non-monotonic shape of the right-hand side accounts for the biphasic behavior of the load-velocity curve in Fig. 4.

The unique steady-state solution of the model lies at the intersection of the two curves in Fig. 2: $v \approx 13.8$; thus the beads move in the ''fast'' regime. The predicted propulsion rate is $V = V_0 \cdot v \approx 70$ nm/s. This compares well with the range of velocities 40–120 nm/s recorded in the experiments (Cameron et al., 2001). Formulae 8 allows us to estimate the effective dissociation rate, $\delta \approx 3$/s, and the force of attachment $f_a \approx 23$ pN (i.e., $\omega(v = 13.8) \approx 0.165$). Thus the molecular links between the attached filaments and the surface break six times faster when the bead moves fast than when the movement is slow. From this we can estimate the ratio of the numbers of working and attached filaments: $w/a = \delta/\kappa \approx 6$. This estimate implies that the average load force per working filament is $f_w \approx f_a \cdot (a/w) \approx 3.8$ pN.

In addition, the following predictions emerge from the model. Cameron et al. (2001) observed that ~10 filaments have their barbed ends in the vicinity of the bead surface. The model predicts that just a few (sometimes one, but rarely zero) filaments are associated with the bead's surface at any one time. The rest of the filaments are generating the propulsive pressure. Their radius of curvature can be estimated as 10–100 nm (a force ~4 pN bends a filament ~4 pN/0.1 pN/nm ~40 nm; this corresponds to a curvature ~100 nm for a filament 150-nm long). Some of these bent filaments straighten out when they are capped and lose contact with the bead surface, but other filaments can be cross-linked by actin-binding proteins, which would ''lock in'' their curvature. This could explain the observation of the ''twisted'' cross-linked filaments, the curvature of which compares favorably with our estimate (Cameron et al., 2001).

Density of coating and percent of extract do not affect velocity

Cameron et al. (2001) noticed that the rate of movement of the ActA-coated beads depends weakly on the degree of dilution of the cytoplasmic extract. Earlier, Cameron et al. (1999) observed that this rate does not depend on the percentage of the bead's surface coated with ActA. This can be explained in the framework of our model as follows. In the absence of the external load, which is the case for the beads, when the viscous load is negligible, Eq. 13 does not depend on the nucleation rate, n. (Only parameter ε_4 depends on n, but this parameter is proportional to $F_L \approx 0$.) Biologically, both the number of working filaments, w, and the number of attached filaments, a, are proportional to the nucleation rate.

Effectively, they work against each other, so the force per filament and resulting velocity are determined by the ratio w/a, and are independent of n. Either ActA on the surface, or Arp2/3 in the cytoplasmic extract, or both, could be rate limiting agents for the nucleation rate, but their respective concentrations would not affect the rate of propulsion. Very weak dependence of the velocity on the degree of dilution of the cytoplasmic extract (Cameron et al., 2001) could be explained by the influence of the G-actin concentration.

Smaller beads move slower

Cameron et al. (1999, 2001) observed that 0.2-μm beads move slower than 0.5-μm beads. This can be understood as follows. Working filaments lose contact with the bead's surface in two ways: first, because they become capped and stop growing, although capping is stochastic so some filaments may grow quite long. Second, most of the filaments are not aligned in the direction of movement, so they eventually grow obliquely enough to ''slip by'' the bead surface before they are capped (Fig. 3). For these filaments the effective rate is limited not by the capping rate, but by their orientation with respect to the load surface. The order of magnitude of this rate can be estimated as $\sim V/r$, where r is the radius of the bead. For a 0.5-μm bead, $V/r = (100\ \text{nm/s})/(250\ \text{nm}) = 0.4/\text{s} < \kappa$, whereby capping is the rate-limiting process. On the other hand, for a 0.2-μm bead, $V/r = (60\ \text{nm/s})/(100\ \text{nm}) = 0.6/\text{s} > \kappa$, so the geometric factor determines the rate at which the working filaments are lost. For very small beads ($V/r > \kappa$), the effective loss rate of working filaments increases in inverse proportion to their radius. At the same time, the dissociation rate is independent of the bead size. Therefore, the ratio of the numbers of working and attached filaments equals the ratio of the dissociation-to-loss rates, and decreases in proportional to the bead radius. Thus smaller beads move more slowly than larger beads.

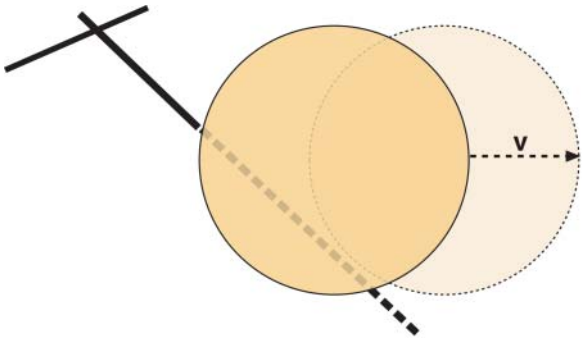

FIGURE 3 The effect of bead size on velocity. Initially, the actin-working filament (*solid line*) is in contact with the bead surface. As the bead moves forward and the filament grows, the filament (*dashed line*) eventually grows past the surface and no longer contributes to the propulsion force.

The force-velocity relation for *Listeria* is biphasic

We computed the force-velocity relation for bead and *Listeria* by solving Eq. 12 using the same values of the model parameters as discussed above ($\varepsilon_1 \approx 5.4$, $\varepsilon_2 \approx 105$, $\varepsilon_3 \approx 0.5$), and varying the external load, F_L, from 0 to 200 pN in increments of 1 pN. Unlike the zero-load case, the nucleation rate influences the cell behavior. We used the value $n = 10/\text{s}$ (at $F_L = 100$ pN corresponding to $\varepsilon_4 \approx 3$); this corresponds to $w = n/\kappa = 20$ working filaments, which is load-independent. The number of attached filaments increases from $a = \text{n}/\delta \approx 3$ at zero load when $\delta \approx 3/\text{s}$, to $a \approx 20$ near stall, when $\delta \approx 0.5/\text{s}$. Together with capped filaments, the total number of filaments is tens to hundreds.

The predicted force-velocity relation is plotted in Fig. 4, showing a peculiar biphasic force-velocity relation: at small loads, the velocity decreases very fast, from 60–70 nm/s, to 10–20 nm/s, as the load grows from 0 to ~20 pN. At greater loads, from ~20 pN to ~200 pN, the velocity decreases slowly with load. Our explanation for this phenomenon is as follows. At small loads, when the bacterial cell moves in the ''fast' regime, the attachments break quickly, and the resistance from the attachments is small. However, at large loads when the bacterium is slowed, the filaments stay attached longer. This increases the effective drag and slows the cell down further. This positive feedback decreases the rate of motion very quickly as the load grows. At still greater loads, there is a crossover to the regime of slow motion where the attachments break with the free dissociation rate, and the force per attachment decreases as the velocity decreases. In this regime, most of the resistance comes from the external load, versus the case of fast motion where significant resistance from the attached filaments amplifies the effect of the viscous load. Consequently, the velocity of a slowly moving cell decreases slowly as the external load grows.

Force-velocity dependence on the tail density

Our model predicts that under the same (nonzero) external load, the velocity is faster if the actin density is greater, and that the actin density of the tail increases with the load, as shown in Figs. 4 and 5. The dashed curve in Fig. 4 is the force-velocity relation computed by solving Eq. 12 with the same model parameters as above, but increasing the nucleation rate threefold to 30/s corresponding to a threefold increase in the number of filaments. The explanation for the observation is simply that the force balance between working and attached filaments is unaffected by the total number of filaments. However, as the total number of filaments grows, the number of working filaments increases, so that the external load per working filament is less. Thus the filaments can grow faster against a smaller total force. Note that at zero load the velocity does not depend on the tail density.

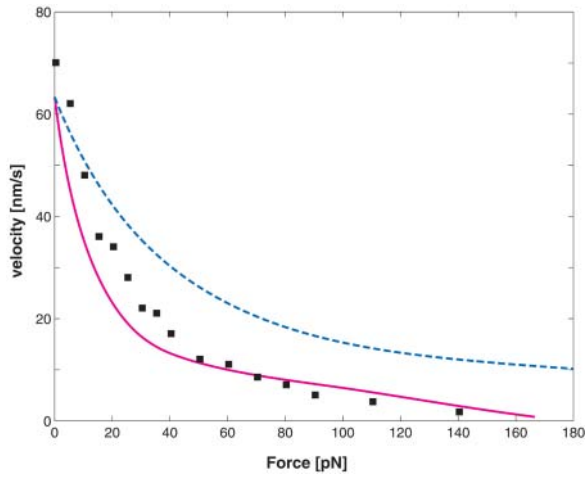

FIGURE 4 The load-velocity curve for *Listeria*. The solid and dashed curves are computed from the deterministic model. The solid curve corresponds to the parameter values in Table 2. The dashed curve corresponds to a threefold increase in nucleation rate over the solid curve, and illustrates the effect of filament density on the load-velocity behavior. The squares represent the data from the stochastic model simulations corresponding to the parameter values in Table 2, other than $V_{max} = 240$ nm/s.

At constant nucleation rate, the number of actin filaments increases with the load (Fig. 5) because of the following mechanism. The average number of working filaments is load-independent, because it is equal to the ratio of the nucleation and capping rates, both of which are constant. On the other hand, the number of the attached filaments is equal to the ratio of the nucleation and dissociation rates, the latter being velocity dependent. When the load grows, then the velocity decreases, which diminishes the effective dissociation rate. Consequently, the attached filaments dissociate slower, and their number increases with the load (Fig. 5). Quantitatively, our model predicts significant (tens of percent) increase in the number of working filaments, as the load grows. These specific model predictions can be tested in future experiments.

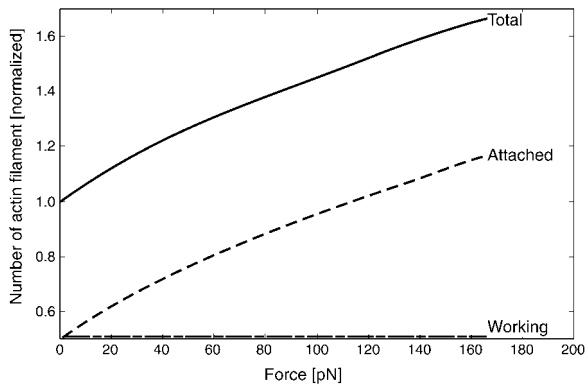

FIGURE 5 Mean field model simulations relating load force to filament density. The number of filaments is normalized to unity at zero load. The solid curve is the number of filaments predicted by the continuous model at varying loads. The dashed curves illustrate that the number of working filaments (*horizontal line*) is independent of the load, whereas the average number of attached filaments increases with the load.

STOCHASTIC MODEL

The number of filaments in the vicinity of the surface of the ActA-coated beads is small enough to make stochastic effects important. To investigate these effects, we simulated the stochastic version of the model. In addition to the continuous model variables, at each time step we compute the extension $x_j(t)$ of the molecular link between the j^{th} attached filament and the surface, $j = 1,\ldots,a(t)$.

In this model, the following events are computed at each time step ($\Delta t = 0.01$ s):

- A new attached filament is nucleated in a stress free state ($x_{a(t)+1} = 0$) with probability $n\cdot\Delta t$.
- Each of the existing attached filaments is detached with probability $\delta_j(t)\cdot\Delta t$, $j = 1,\ldots,a(t)$. The rate of detachment is computed as $\delta_j(t) = \delta_0\cdot\exp[f_j(t)/f_b]$. The force applied to the corresponding link is found using the Hook's law: $f_j(t) = k\cdot x_j(t)$.
- Each of the existing working filaments is removed with probability $\kappa\cdot\Delta t$.
- The number of the working filaments, $w(t + \Delta t)$, is increased by the number of the filaments just being detached.
- The force per working filament is calculated by adding up the attachment forces, including the external load, and dividing the result by the number of working filaments:

$$f_w = \left(F_L + \sum_{j=1}^{a(t+\Delta t)} f_j(t)\right)/w(t+\Delta t).$$

- The velocity is calculated using the formula: $V = V_{max}\exp\{-f_w\ell/k_BT\} - V_{dep}$.
- The coordinate of the load and all of the extensions $x_j(t)$, $j = 1,\ldots,a(t + \Delta t)$ of the molecular links are increased by $V\cdot\Delta t$.

The results of the simulations of this model are shown in Fig. 6 for zero external load. The same model parameters as those used in the deterministic model were used in the simulations, with one exception described below.

The simulations reveal that, because of the fluctuations in the number of the filaments and the nonlinearity of the force-velocity relations for the actin filaments, the average velocity predicted by the stochastic model is greater than predicted by the deterministic theory. The reason for this difference is that, from time to time, the number of attached filaments fluctuates down to one or two, or even zero. (The time intervals are too short for the bacterium or bead to drift away when $a = 0$). In these time intervals, the working filaments grow with a rate close to the free polymerization velocity. The average effect is greater than the cumulative slowing

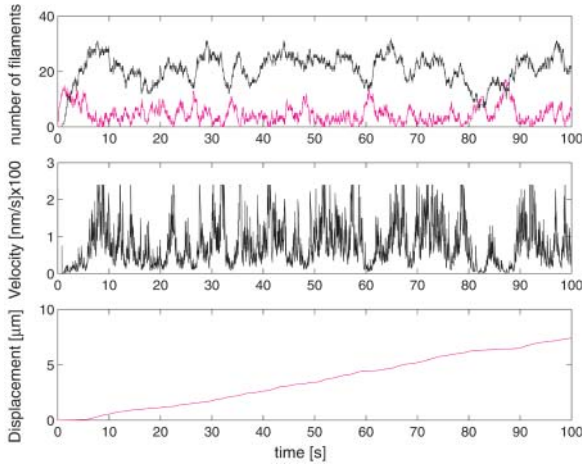

FIGURE 6 Simulations of the stochastic model. In all three graphs the x axis is time in seconds. (*Top*) Upper and lower curves show the numbers of working and attached filaments, respectively. (*Middle*) Velocity in nanometers per second ($\times 100$). (*Bottom*) Cumulative distance traveled in microns.

down due to opposing fluctuations that increase the number of attachments. Thus the model predicts the observed rate of propulsion, $V \approx 70$ nm/s, at $V_{max} = 240$ nm/s, about half of the value used in the deterministic model (although still within the biological range of G-actin concentrations). The simulations give the following average values for the numbers of filaments and corresponding forces: $w \approx 20$, $a \approx 4$, $f_a \approx 15$ pN, and $f_w \approx 3$ pN; these are of the same order as those obtained in the continuous model. Simulations at various values of the external load demonstrate that the stochastic model gives a force-velocity relation close to the one obtained from the deterministic model (Fig. 4).

Although the velocity fluctuations are large, because of the large relative fluctuations of the small number of attached filaments, these fluctuations are very frequent. Thus the resulting distance versus time trajectory is relatively smooth, as observed. Simulations with lower nucleation rate (not shown) predict greater fluctuations in the trajectory, and give the average total number of filaments ~ 10 similar to that observed in the experiments with plastic beads (Cameron et al., 2001).

Symmetry breaking through the cloud of actin

Cameron et al. (1999) observed that an ActA-coated plastic bead, after polymerizing a dense actin network around itself, would then ''break through'' the actin network and propel itself directionally with the actin tail behind the bead. Using BR theory, van Oudenaarden and Theriot developed a two-dimensional stochastic model that relied upon force-dependent actin depolymerization to generate stochastic instability. Effective diffusion coefficients increase dramatically and was interpreted as the onset of symmetry breaking (van Oudenaarden and Theriot, 2000). Rather than altering depolymerization, our stochastic model assumes that forces alter the rate of cross-link dissociation between actin filaments. Our model demonstrates similar symmetry-breaking behavior.

Consider the one-dimensional situation shown in Fig. 7, where two opposing populations of filaments drive an object: one to the left, and one to the right. We simulate both filament populations simultaneously as described above. The forces generated by the two ''tails'' almost balance so that the object is nearly stalled, trapped in the cloud of actin. However, occasionally the number of filaments on one side of the load fluctuates down so much that the filaments on the other side gain the advantage and start to push the load. If the filament population on the depleted side is not quickly replenished, then the unidirectional movement will become irreversible. We model the abrupt transition to the unidirectional model as follows.

The filaments with barbed ends near the surface of the object are cross-linked into the polymer network around the object. We treat these cross-links as dynamic attachments with the same mechanical properties as those of the bonds between the actin filaments and the surface. We assume that the cross-links are generated by each filament near the surface at the rate $n_c = 1$/s, and then dissociate with a rate that increases with the elastic force. We assume that the total elastic force from the bent working filaments is equipartitioned between all existing cross-links. Then, the following

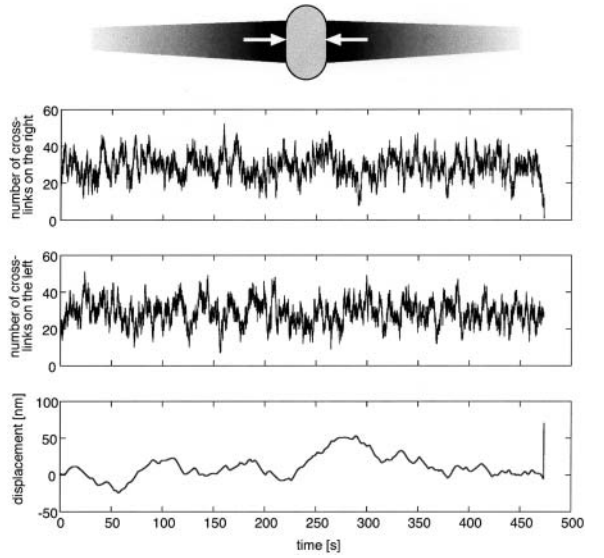

FIGURE 7 Results of the stochastic model simulations where the filaments grow at the left and right of a bead. In all three graphs, the x axis is time in seconds. (*Top panel*) Number of cross-links on the right. (*Middle panel*) Number of cross-links on the left. (*Bottom panel*) Cumulative distance traveled in nanometers. The bead undergoes an unbiased random walk for almost 500 s, whereupon the number of cross-links at the right fluctuates to zero, whereas the filaments at the left overcome the resistance of the attached filaments, and the bead breaks through the cloud of actin and commences unidirectional motion to the left.

positive feedback mechanism leads to symmetry breaking, whereby the bead moves convectively in one direction or the other. If, for example, the total number of filaments fluctuates down on the right, then fewer cross-links are generated at that side and a significant force is applied to each of these cross-links. According to Evans' theory, they break faster, which distributes the same force among an even smaller number of cross-links, further accelerating their dissociation (Evans, 2001; Evans and Ritchie, 1999). Eventually, a fluctuation will arise wherein there will be no cross-links on one side, and the object can then be pushed rapidly by the working filaments on the other side.

In order to simulate such an event, we compute the dynamics on the left and right as described in the previous section. The two processes are independent, except for the forces generated and the velocity of the object, which are computed using the balance of forces from both sides. In addition:

- A new cross-link is nucleated at each side with respective probability $n_c^{r,l}\cdot\,\Delta t$: $n_c^{r,l} = (a(t) + w(t))|_{\text{right, left}}$.
- Each of the existing cross-links is detached with probability $\delta_c^{(r,l)}(t)\cdot\Delta t$, $j = 1,\ldots,c_{r,l}(t)$, where $c_{r,l}$ is the number of cross-links on the right and left, respectively. The rate of detachment is computed as $\delta_c^{(r,l)}(t) = \delta_0\cdot\exp[f^{r,l}(t)/f_b]$. The force applied to the corresponding cross-link is found as $f^{r,l}(t) = F/c_{r,l}$, where F is the magnitude of the total force applied to the object from the right (or left: the forces balance).
- The computations are stopped when the number of the cross-links at either side is zero, after which the movement is simulated for a short time interval using just the actin dynamics at the opposite side.

The results of the simulations are shown in Fig. 7 for the same model parameters as in the previous simulations. The symmetry break takes place after ~500 s. Simulations with greater values of the nucleation rate show that the symmetry break occurs on the average after a much longer time. This can be explained by the fact that greater filament numbers mean fewer relative fluctuations, so there are always enough filaments on each side to resist the force of protrusion. Some features of this model are analogous to the observed phenomena: the directed movement starts only after an asymmetric buildup of actin density near the bead surface. Also, the frequency of the symmetry break is greater if either the bead size is smaller, or the cytoplasmic extract is more diluted (Cameron et al., 1999, 2001), corresponding to attenuation of the nucleation rate. Of course, these simulations merely illustrate the phenomenon. A much more detailed three-dimensional stochastic simulation is required, taking into account the geometry of the actin network and elasticity effects. However, we note that the origin of the symmetry breaking in our model is different from that modeled by van Oudenaarden and Theriot (2000).

DISCUSSION

The question we have addressed here is the physical mechanism for propulsion of pathogenic bacteria, such as *Listeria* and *Shigella*. That is, what is the nature of the propulsion force? EBR models posit that actin polymerization alone is responsible for the respective force generation. Recently, it has been established that the cells are connected to their actin tails, so how can there be the required microscopic gap between the filaments and the surface? Our answer is that filaments nucleate attached to the surface, but soon they detach from the cell and generate force according to the EBR model. The attached fibers are under tension and the working filaments are in compression. Some of the working filaments bend and cross-link, so they are locked in a bent configuration. Although the attached filaments hinder propulsion, they stabilize movement by maintaining contact between the bacterium and its actin tail.

We assume that actin fibers are nucleated in the attached state. Then, they detach and push the bacterial cell forward until capping removes the growing barbed ends from the proximity of the bacterial surface. Because of this assumption, both pushing and resisting populations of filaments are proportional to the nucleation rate, although their ratio does not depend on this rate. This accounts for the independence of the rate of movement on the degree of ActA coating or the dilution of cytoplasmic extracts in experiments (Cameron et al., 1999, 2001). On the other hand, at high external loads, the more filaments in the tail, the less is the load per filament, and the faster is the propulsion. The model also explains why smaller ActA-coated beads move more slowly: growing barbed ends slip off the small bead's surface faster before they are capped. This effectively decreases the number of the working filaments without changing the number of attached filaments, which weakens the propulsion force.

By collecting known model parameters from the literature, estimating the unknown parameters from available data, and analyzing the F-actin dynamics and force balance between the attached and detached filaments, we estimate the rate of propulsion of *Listeria* and ActA-coated plastic beads. The model predicts the value of the velocity of the order of tens of nanometers per second, which is within the observed range. When an external load is applied to the cell, the model predicts the biphasic load-velocity relation. The explanation is based on Evans' theory of weak molecular bonds (Evans and Ritchie, 1999): when the movement is fast, an external load helps the attachment filaments to hold on longer, thus increasing the effective resistance and slowing the movement further. When the propulsion is slow, the external load has little effect on the weak internal actin resistance, and the velocity decreases slowly with the load.

Stochastic model simulations demonstrate that fluctuations in the propulsion rate grow as the density of the actin tail decreases, due to greater relative fluctuations of the

numbers of attached and pushing filaments. These simulations also illustrate how a bead trapped in an actin cloud breaks through and commences unidirectional movement.

Some of the model predictions conform to the existing data; others can be tested. For example, fluctuations in the velocity and their correlation with tail density can be quantified and compared with the stochastic model simulations. Systematic measurements of the force-velocity relations at different tail densities also can be compared to the theoretical results. Time-lapse microscopy and fluorescence resonance energy transfer technique could be used to observe the processes of filament dissociation and pushing simultaneously with recording the progress of a bead. If the capping protein concentration is changed, as in the experiments of Loisel et al. (1999), and more bead sizes are tried, then the model can be used to predict the dependence of the velocity on the capping rate and bead size.

Finally, the model predicts that a force of ~20 pN per attached filament (or a total force of tens of piconewtons for the bead, and hundreds of piconewtons for the cell) is necessary to separate the bead or cell from the actin tail. It may be possible to measure this detachment force in experiments similar to those of Theriot and van Oudenaarden with ActA-coated lipid vesicles.

Implications for the protrusion at the leading edge of the crawling cell

In this work, we considered movements powered by growing actin tails. The actin machinery at the leading edge of the motile cells is considerably more complex. As we discussed in the Introduction, the molecular players may be different in the lamellipodia. However, our model has implications for the protrusion in the crawling cells. Abraham et al. (1999) observed that the total number of actin filaments at the leading edge of the lamellipod is ~250/μm of the leading edge. Assuming that the same model parameters apply, the ratio of the working to attached filaments, $w/a \sim 6$, so $a \sim 30$–$40/\mu$m, $w \sim 200/\mu$m. Then, total pushing and resistance forces, which are balanced, $f_w \cdot w = f_w \cdot w \sim 4$ pN$\cdot 200/\mu$m ~ 800 pN/μm. This figure is in the same range as the experimental estimates of Dai and Sheetz (1999), who reported forces of hundreds of piconewtons per micron required to break attachments between the actin cortex and cell membrane. Note that the additional resistance from bending the cell membrane at the leading edge is negligible in comparison, ~35 pN/μm (Evans and Skalak, 1979). Extrapolating the results on the force-velocity relations to lamellipodial protrusion (the leading edge is ~10–30-μm long), we can predict that stalling forces of hundreds of piconewtons would slow the protrusion significantly, whereas at forces in the nanonewton range, the slow protrusion would persist almost independently of the force. Of course, at the present state of knowledge, it is very hard to make predictions about the crawling cell, where conditions vary significantly from cell to cell, and the details of the actin network organization are poorly understood.

Open questions

A detailed microscopic model of actin-based force generation is still pending. Here we have modeled on a microscopic level, including as many molecular details as possible. Eventually the rates and concentrations of the molecular players near the cell surface will be known, and that will allow us to refine the model. However, the model is adequate for a relatively stiff actin network. In the case of softer networks, our model could serve as a boundary condition for a mesoscopic elastic model of the actin tail (see Gerbal et al., 2000). Our model in its present form cannot explain the discrete character of bacterium advancement in steps of 5.4-nm observed by Kuo and McGrath (2000). We discuss this phenomenon from the viewpoint of the model in the Appendix. More research is necessary to assess the importance of three-dimensional effects on stress distributions in the actin network near a curved cell surface. Particularly, extension of our model to 3-D stochastic simulations, perhaps of Monte Carlo type (Carlsson, 2001), is necessary to make more accurate predictions.

APPENDIX A: AUTOCATALYTIC ACTIN BRANCHING DYNAMICS

In the more specific, modified, version of the model, the dynamics of the two filament populations obey the following system of equations.

$$\text{Attached filaments: } \frac{da}{dt} = \underset{\text{Association}}{n} - \underset{\text{Dissociation}}{\delta \cdot a}. \tag{13}$$

$$\text{Working filaments: } \frac{dw}{dt} = 2 \cdot \underset{\text{Dissociation}}{\delta \cdot a} - \underset{\text{Association}}{n} - \underset{\text{Capping}}{\kappa \cdot w}. \tag{14}$$

This system of equations describes the following autocatalytic branching mechanism (M.F. Carlier, personal communication). Working filaments attach to the surface with the rate n. (For simplicity, we assume that this rate is limited not by the number of the working filaments, but by activity of ActA, so n is the constant model parameter independent of w.) Each such act decreases the number of working filaments by one, and increases the number of the attached filaments by one (see ''association'' terms in Eqs. 13 and 14). Upon association, Arp2/3 complex associates with the interface between the surface and the barbed ends and nascent actin filament is nucleated (branches out at this interface). This complex dissociates with the rate δ. At this moment, the number of the attached filaments decreases by one (''mother'' filament), whereas the number of the detached, working filaments increases by two (both ''mother'' and ''daughter'' filaments; see ''dissociation'' terms in Eqs. 1 and 2). Finally, the working filaments are capped with the rate κ.

We investigate the model's behavior in the case of the steady propulsion with a constant rate. From the first equation, we have $a = n/\delta$. Substituting this into the second equation, we obtain $w = (1/\kappa)(2\delta a - n) = (1/\kappa)(2n - n) = n/\kappa$. Thus, in this model, the steady-state solutions of Eqs. 13 and 14) are the same as in our simple model.

APPENDIX B: APPROXIMATIONS ABOUT THE SEQUENCE OF MOLECULAR EVENTS NEAR THE SURFACE

The model equations are based on the implicit assumption that when an attached filament dissociates, the filament (or, in the autocatalytic scenario, two filaments) immediately becomes a working filament. In fact, before the dissociation, the tip of the attached filament is most likely pulled forward by the advancing surface of the bead/bacterium. Thus, upon the dissociation, the filament's tip springs back, and it takes time for it to catch up with the surface. However, this time is very small. Indeed, when the tip is out of touch with the surface, it grows with the free net polymerization rate, unattenuated by the force. This rate is hundreds of nanometers per second, whereas the distance the tip has to advance before engaging the surface is tens of nanometers. Therefore, catch-up would take on the order of a tenth of a second; this is negligible compared to the average time before capping, and our assumption does not introduce a significant error.

Another implicit assumption is that upon nucleation/branching, the effective flexible spring can be characterized by a single elastic constant k. This is a stronger assumption. In fact, at the moment of branching, the ''mother'' filament is most likely bent only slightly. Then, for a time of order 1 s (10's nm/10's nm/s) the filament is bent. During that time, the effective spring constant associated with this bending is of the order of a few tenths pN/nm (0.1 pN/nm for a filament 200-nm long, more than that for more abundant shorter filaments). After that, the filament is pulled taut in the direction of movement. The corresponding spring constant associated with the longitudinal pulling of F-actin is large, of the order of hundreds of pN/nm. In this state, the effective spring constant is determined by i), the protein elasticity of the links between actin filament, ii), the surface, iii), interactions between filaments, or, more likely, iv), the elasticity of other filaments cross-linked into actin tail meshwork,. This constant is likely to be of the order of 10 pN/nm. Precise calculation of the force-velocity curve that takes into consideration this sequence of events requires 3-D Monte Carlo simulations of an actin network. Though possible in principle, such computations would not have the clarity and simplicity of our model. Therefore, we approximate the complex dynamic elasticity of the effective molecular links with a constant linear Hook's law. We use the elastic constant that is likely to lie in between the ''slightly bent filament'' regime and the ''pulled taut filament'' regime, $k = 1$ pN/nm. At the same time, this constant has the same order of magnitude as the characteristic protein elasticity constant (Howard, 2001). This is hard to prove quantitatively, but the qualitative conclusions of our model are unlikely to change because of this approximation. Future computational modeling will test the validity of the approximation.

APPENDIX C: NUMERICAL SOLUTION OF EQ. 12

The function $f(v)$ on the right-hand side of Eq. 12, $v = f(v)$, has the following properties: i), $f(0)$ is a finite positive number; ii), $f(v)$ has a single positive minimum, $f(0) > f(v_1) > 0$; iii), $f(v)$ has a horizontal asymptote, $f(v) \rightarrow \text{const} > f(v_1)$, as $v \rightarrow \infty$; iv), $f(v)$ decreases at $0 < v < v_1$, and increases at $v > v_1$; and v), $f(v)$ is concave up at $0 < v < v_2$, and down at $v > v_2$, where $v_2 > v_1$. It is easy to show that these properties ensure that Eq. 12 has either one or three solutions, depending on the model parameters. Systematic numerical plotting demonstrates that over a wide range of biologically relevant parameters, there is a single solution of Eq. 12. An approximate solution was found numerically and used as the starting point of the bisection algorithm (unconditionally converging), which determined the unique solution with a specified precision.

APPENDIX D: IS THE TETHERED RATCHET MOTOR A "STEPPER"?

Kuo and McGrath (2000) observed that *Listeria* advances in discrete steps. The measured step size was in the nanometer range. Steps of much larger scale are observed in movement of beads (Bernheim-Groswasser et al., 2002) and vesicles (van Oudenaarden, personal communication). These steps are a macroscopic phenomenon most likely related to the rheology of the actin tail and its interface with the surface, and so not relevant at the microscopic scale. Kuo and McGrath (2000) observed that the most frequent step size was ~5.5 nm, similar to the size of an actin monomer. Moreover, the variance of the step size was very small, in the subnanometer range. The steps could indicate some intrinsic molecular scale mechanism at the interface between filaments and the surface. Here we investigate whether our model can address the nature of the microscopic steps.

If the number of the attached filaments is small, breaking one of the attachments focuses stress on the rest of the attached filaments. For example, if five filaments are attached, and the average force per attached filament is ~20 pN, then breaking one of the attachments increases the force on each of the remaining attachments by ~5 pN. This stretches the associated links by ~(5 pN)/(1 pN/nm) ~ 5 nm. Consequently, the cell appears to make a forward step of this length.

To make this argument more precise, we simulated the stochastic model with the same parameters given in Table 2. Each time an attachment breaks, we compute the discrete forward step using the formula: $\Delta x = F(t)/k(1/a(t) - (1/a(t - \Delta t)))$. Here F is the total force applied to the cell by the working filaments, which does not differ significantly from step to step. The simulations showed that the cell advanced in steps of ~2–3 nm, albeit with significant variations in step size due to the large fluctuations in the number of filaments. The average step size depends on the capping and dissociation rates, and on the spring constant. For example, when we decreased the capping rate to $\kappa = 0.3$/s, and decreased the spring constant to $k = 0.5$ pN/nm, the model gives the most frequent step size ~3–4 nm. In this case, we calculated the histogram shown in Fig. 8. It exhibits a broad distribution of step sizes, with an average of ~5 nm, which is larger than the most frequent step size (~3–4 nm). Simulations also show that the step size depends only weakly on the nucleation rate, n.

This explanation depends on the fluctuating number of attached filaments and the mechanical properties of the attachments, so the similarity of the step and monomer sizes is coincidental. If this explanation is correct, the step size should be different in experiments with plastic beads, where essential rates and concentrations could differ from those in experiments with *Listeria*. This can be tested. One of the predictions is that there is a correlation between step sizes in time. For example, when the number of attached filaments is small, the step size is large, but then the next step is also likely to be large. Conversely, with greater number of attached filaments, the consecutive steps would all be small. This prediction could also be tested.

Finally, Kuo and McGrath (2000) estimated that the effective spring constant of the combined links between the actin tail and bacterium is ~40 pN/nm. Our estimates are of the same order of magnitude, but lower, ~10 pN/nm. The model is accurate only to an order of magnitude, so this cannot be considered a serious discrepancy. However, the model's prediction of the

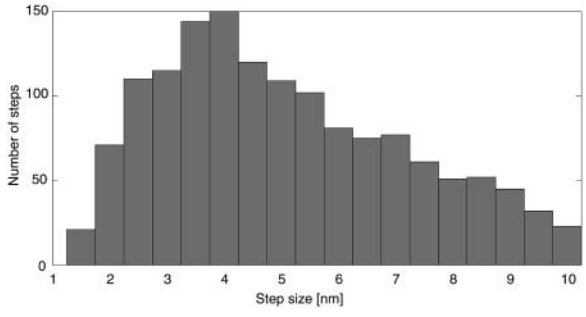

FIGURE 8 Results of the stochastic model simulations with the model parameters described in the text giving the histogram of step-size frequency. The most frequent step size is ~3–4 nm.

broad distribution of the step size sensitive to geometric and kinetic factors disagrees with the data as presented in Kuo and McGrath (2000) and the theoretical predictions of Dickinson and Purich (2002). More detailed modeling and experiments could address this issue, as well as alternative explanations for the stepping behavior.

Note added in proof: Since submission of this manuscript, McGrath et al. (2003) used methylcellulose to vary the viscosity and measured the viscous drag force applied to Listeria. The measured load-velocity relation agrees very well with our model prediction, both qualitatively (biphasic dependence), and quantitatively. They also observed that the tail actin density increased with the load, which also conforms with the theoretical prediction of the model. Similar measurements of another group, however, produced a velocity of propulsion largely independent of the force up to loads of hundreds of piconewtons (S. Wiesner, E. Helfer, D. Didry, G. Ducouret, F. Lafuma, M.-F. Carlier, and D. Pantaloni. 2003. *J. Cell Biol.* 160:387–398). If the number of actin filaments in these experiments is much greater than in the McGrath et al. experiments, than the forward thrust of many working filaments balances largely by the resistance from many attached filaments, so that the external load changes this balance very little. Hence the velocity insensitive to the load (see the *dashed curve* in Fig 4).

We thank N. London for M.-F. Carlier, the help at early stages of this work, and S.C. Kuo, A. van Oudenaarden, and J. Theriot for useful discussions and sharing unpublished experimental data. A.M. is grateful to the Isaak Newton Institute for Mathematical Sciences, University of Cambridge, where part of this work was done.

A.M. is supported by a University of California at Davis Chancellor's Fellowship, National Science Foundation award DMS-1097746, and a National Institutes of Health Glue Grant ''Cell Migration Consortium'' National Institute of General Medical Sciences U54 GM64346. G.O. is supported by National Institutes of Health award GM59875-02 and National Science Foundation award DMS-9972826.

REFERENCES

Abraham, V. C., V. Krishnamurthi, D. L. Taylor, and F. Lanni. 1999. The actin-based nanomachine at the leading edge of migrating cells. *Biophys. J.* 77:1721–1732.

Bear, J. E., M. Krause, and F. B. Gertler. 2001. Regulating cellular actin assembly. *Curr. Opin. Cell Biol.* 13:158–166.

Beckerle, M. C. 1998. Spatial control of actin filament assembly: lessons from Listeria. *Cell.* 95:741–748.

Bernheim-Groswasser, A., S. Wiesne, R. Golsteyn, M. F. Carlier, and C. Sykes. 2002. The dynamics of actin-based motility depend on surface parameters. *Nature.* 417:308–311.

Borisy, G. G., and T. M. Svitkina. 2000. Actin machinery: pushing the envelope. *Curr. Opin. Cell Biol.* 12:104–112.

Boujemaa-Paterski, R., E. Gouin, G. Hansen, S. Samarin, C. L. Clainche, D. Didry, P. Dehoux, P. Cossart, C. Kocks, M. F. Carlier, and D. Pantaloni. 2001. Listeria protein ActA mimics WASP family proteins: it activates filament barbed end branching by Arp2/3 complex. *Biochemistry.* 40:11390–11404.

Bray, D. 2001. Cell Movements, 2nd ed. Garland, New York.

Cameron, L. A., M. J. Footer, A. van Oudenaarden, and J. A. Theriot. 1999. Motility of ActA protein-coated microspheres driven by actin polymerization. *Proc. Natl. Acad. Sci. USA.* 96:4908–4913.

Cameron, L. A., P. A. Giardini, F. S. Soo, and J. A. Theriot. 2000. Secrets of actin-based motility revealed by a bacterial pathogen. *Nat. Rev. Mol. Cell Biol.* 1:110–119.

Cameron, L. A., T. M. Svitkina, D. Vignjevic, J. A. Theriot, and G. G. Borisy. 2001. Dendritic organization of actin comet tails. *Curr. Biol.* 11:130–135.

Carlsson, A. E. 2001. Growth of branched actin networks against obstacles. *Biophys. J.* 81:1907–1923.

Condeelis, J. 1993. Life at the leading edge: the formation of cell protrusions. *Annu. Rev. Cell Biol.* 9:411–444.

Cortese, J. D., B. Schwab 3rd, C. Frieden, and E. L. Elson. 1989. Actin polymerization induces a shape change in actin-containing vesicles. *Proc. Natl. Acad. Sci. USA.* 86:5773–5777.

Dai, J., and M. P. Sheetz. 1999. Membrane tether formation from blebbing cells. *Biophys. J.* 77:3363–3370.

Dickinson, R. B., and D. L. Purich. 2002. Clamped filament elongation model for actin-based motors. *Biophys. J.* 82:605–617.

Egile, C., T. P. Loisel, V. Laurent, R. Li, D. Pantaloni, P. J. Sansonetti, and M. F. Carlier. 1999. Activation of the CDC42 effector N-WASP by the Shigella flexneri IcsA protein promotes actin nucleation by Arp2/3 complex and bacterial actin-based motility. *J. Cell Biol.* 146:1319–1332.

Evans, E. 2001. Probing the relation between force—lifetime—and chemistry in single molecular bonds. *Annu. Rev. Biophys. Biomol. Struct.* 30:105–128.

Evans, E., and K. Ritchie. 1999. Strength of a weak bond connecting flexible polymer chains. *Biophys. J.* 76:2439–2447.

Evans, E. A., and R. Skalak. 1979. Mechanics and thermodynamics of biomembranes: part 1. *CRC Crit. Rev. Bioeng.* 3:181–330.

Gerbal, F., P. Chaikin, Y. Rabin, and J. Prost. 2000. An elastic analysis of Listeria monocytogenes propulsion. *Biophys. J.* 79:2259–2275.

Hill, T. L., and M. W. Kirschner. 1982. Bioenergetics and kinetics of microtubule and actin filament assembly-disassembly. *Int. Rev. Cytol.* 78:1–125.

Howard, J. 2001. Mechanics of Motor Proteins and the Cytoskeleton. Sinauer, Sunderland, MA.

Kojima, H., A. Ishijima, and T. Yanagida. 1994. Direct measurement of stiffness of single actin filaments with and without tropomyosin by in vitro nanomanipulation. *Proc. Natl. Acad. Sci. USA.* 91:12962–12966.

Kuo, S. C., and J. L. McGrath. 2000. Steps and fluctuations of Listeria monocytogenes during actin-based motility. *Nature.* 407:1026–1029.

Laurent, V., T. P. Loisel, B. Harbeck, A. Wehman, L. Grobe, B. M. Jockusch, J. Wehland, F. B. Gertler, and M. F. Carlier. 1999. Role of proteins of the Ena/VASP family in actin-based motility of Listeria monocytogenes. *J. Cell Biol.* 144:1245–1258.

Loisel, T. P., R. Boujemaa, D. Pantaloni, and M. F. Carlier. 1999. Reconstitution of actin-based motility of Listeria and Shigella using pure proteins. *Nature.* 401:613–616.

Machesky, L. M., R. D. Mullins, H. N. Higgs, D. A. Kaiser, L. Blanchoin, R. C. May, M. E. Hall, and T. D. Pollard. 1999. Scar, a WASP-related protein, activates nucleation of actin filaments by the Arp2/3 complex. *Proc. Natl. Acad. Sci. USA.* 96:3739–3744.

McGrath, J., N. Eungdamrong, C. Fisher, F. Peng, L. Mahadevan, T. Mitchison, and S. Kuo. 2003. The force-velocity relationship for the actin-based motility of Listeria moncytogenes. *Curr. Biol.* In press.

Mitchison, T. J., and L. P. Cramer. 1996. Actin-based cell motility and cell locomotion. *Cell.* 84:371–379.

Miyata, H., S. Nishiyama, K. Akashi, and K. Kinosita Jr. 1999. Protrusive growth from giant liposomes driven by actin polymerization. *Proc. Natl. Acad. Sci. USA.* 96:2048–2053.

Mogilner, A., and G. Oster. 1996. Cell motility driven by actin polymerization. *Biophys. J.* 71:3030–3045.

Noireaux, V., R. M. Golsteyn, E. Friederich, J. Prost, C. Antony, D. Louvard, and C. Sykes. 2000. Growing an actin gel on spherical surfaces. *Biophys. J.* 78:1643–1654.

Olbris, D. J., and J. Herzfeld. 2000. Reconstitution of Listeria motility: implications for the mechanism of force transduction. *Biochim. Biophys. Acta.* 1495:140–149.

Pantaloni, D., C. L. Clainche, and M. F. Carlier. 2001. Mechanism of actin-based motility. *Science*. 292:1502–1506.

Peskin, C., G. Odell, and G. Oster. 1993. Cellular motions and thermal fluctuations: the Brownian ratchet. *Biophys. J*. 65:316–324.

Pollard, T. D., L. Blanchoin, and R. D. Mullins. 2000. Molecular mechanisms controlling actin filament dynamics in nonmuscle cells. *Annu. Rev. Biophys. Biomol. Struct*. 29:545–576.

Rohatgi, R., L. Ma, H. Miki, M. Lopez, T. Kirchhausen, T. Takenawa, and M. W. Kirschner. 1999. The interaction between N-WASP and the Arp2/3 complex links Cdc42-dependent signals to actin assembly. *Cell*. 97:221–231.

Theriot, J. A., T. J. Mitchison, L. G. Tilney, and D. A. Portnoy. 1992. The rate of actin-based motility of intracellular Listeria monocytogenes equals the rate of actin polymerization. *Nature*. 357:257–260.

Tilney, L. G., and D. A. Portnoy. 1989. Actin filaments and the growth, movement, and spread of the intracellular bacterial parasite, Listeria monocytogenes. *J. Cell Biol*. 109:1597–1608.

van Oudenaarden, A., and J. A. Theriot. 2000. Cooperative symmetry-breaking by actin polymerization in a model for cell motility. *Nat. Cell Biol*. 1:493–499.

Welch, M. D., J. Rosenblatt, J. Skoble, D. A. Portnoy, and T. J. Mitchison. 1998. Interaction of human Arp2/3 complex and the Listeria monocytogenes ActA protein in actin filament nucleation. *Science*. 281:105–108.

Yarar, D., W. To, A. Abo, and M. D. Welch. 1999. The Wiskott-Aldrich syndrome protein directs actin-based motility by stimulating actin nucleation with the Arp2/3 complex. *Curr. Biol*. 9:555–558.